

Photo and Redox Dual Responsive Reversibly Cross-Linked Nanocarrier for Efficient Tumor-Targeted Drug Delivery

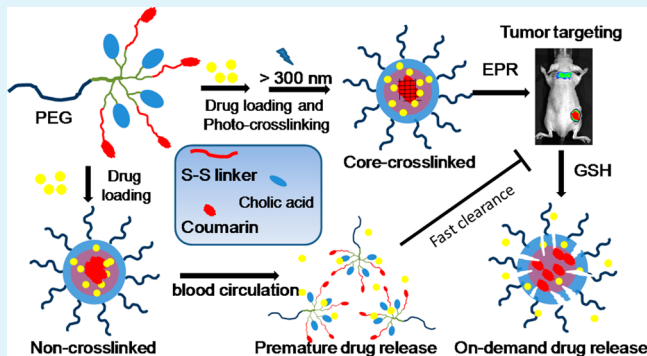
Yu Shao,[†] Changying Shi,[†] Gaofei Xu,^{†,‡} DanDan Guo,[†] and Juntao Luo^{*,†}

[†]Department of Pharmacology, SUNY Upstate Cancer Research Institute, State University of New York Upstate Medical University, Syracuse, New York 13210, United States

[‡]Department of Applied Chemistry, College of Science, China Agricultural University, Beijing, 100193, China

Supporting Information

ABSTRACT: To develop a feasible and efficient nanocarrier for potential clinical application, a series of photo and redox dual responsive reversibly cross-linked micelles have been developed for the targeted anticancer drug delivery. The nanocarrier can be cross-linked efficiently via a clean, efficient, and controllable coumarin photodimerization within the nanocarrier, which simplify the formulation process and quality control prior clinical use and improve the *in vivo* stability for tumor targeting. At the same time, cross-linking of nanocarrier could be cleaved via the responsiveness of the built-in disulfide cross-linkage to the redox tumor microenvironment for on-demand drug release. Coumarin and disulfide bond was introduced into a linear-dendritic copolymer (named as telodendrimer) precisely via peptide chemistry. The engineered nanocarrier possesses good drug loading capacity and stability, and exhibits a safer profile as well as similar anticancer effects compared with free drug in cell culture. The *in vivo* and *ex vivo* small animal imaging revealed the preferred tumor accumulation and the prolonged tumor residency of the payload delivered by the cross-linked micelles compared to the non-cross-linked micelles and free drug surrogate because of the increased stability.



KEYWORDS: cross-linking, photo sensitive, redox sensitive, micelle, drug delivery, dual responsive

INTRODUCTION

Several nanomedicines have been approved by the U.S. Food and Drug Administration (FDA) on the basis of their improved efficacy or reduced toxicity over the parent drugs, for example, stealth liposomal formulations of doxorubicin (Doxil) and the human serum albumin bounded paclitaxel nanoparticle (Abraxane). Furthermore, various nanoparticles have been used for delivering drug molecules to tumors,^{1–3} and several nanotherapeutics have entered into clinical trials worldwide.⁴ Compared with dendrimers, liposomes, and other organic/inorganic nanoparticles, polymeric micelles are much more versatile to deliver a broad spectrum of therapeutics because of their enormous chemical variation, relative easy preparation, multiple functionality, high drug loading capacity, and small particle sizes (10–100 nm).^{5,6} Furthermore, polymeric micelles appear to take advantage of the enhanced permeability and retention effect (EPR effect)^{7,8} in solid tumors to increase drug accumulation at the tumor sites.

The efficient *in vivo* drug delivery via nanocarriers is still very challenging due to the complexity of the physiological and pathological microenvironments.^{9,10} The stability of nanocarriers, especially for polymeric micelles, is critical for the *in vitro* quality control and the *in vivo* efficacy in disease treatment. The premature drug release of the payload drug from

nanocarriers diminishes the outcome of nanoformulations for targeted drug delivery, yielding only marginal improved therapeutic index and toxicity profile. For polymeric micelle nanocarriers, the poor *in vivo* stability is mainly due to the dissociation of micelles under the extreme dilution *in vivo*, as well as the interactions with hydrophobic biological components, for example, plasma membrane, lipophilic proteins, and endogenous lipophilic nanoparticles (HDL and LDL), etc. To overcome this problem, cross-linking strategies have been developed to stabilize drug-loaded micelles.¹¹ Chemical reactions, such as vinyl bond polymerization,^{12,13} amide bond formation,^{14–16} disulfide bond formation,^{17–19} etc., were the most commonly used ways to cross-link polymeric micelles.¹¹ However, most cross-linking techniques possess inherent drawbacks, which potentially hinder their further clinical development, such as irreversibility, poor control, difficulty in monitoring the degree of cross-linking. Furthermore, the extra cross-linking reagents or catalyst are usually added to cross-link drug-loaded micelles. The residues of these toxic small molecules need to be removed via extensive dialysis prior to

Received: March 28, 2014

Accepted: June 12, 2014

Published: June 12, 2014

the *in vivo* application. However, severe concerns would be raised for dialysis process, such as the loss of drug molecules, as well as extra sterilization and quality control. Therefore, it could be foreseen that many of these chemically cross-linked formulations might not be appreciated in pharmaceutical industries, as well as in the clinical practice, because of the drawbacks discussed above. To develop a clean and clinically feasible strategy for nanocarrier cross-linking, Luo and Lam et al. have synthesized a reversible disulfide-bond cross-linked micelle via molecular oxygen oxidation.^{20,21} To target tumor microenvironment for on-demand drug release in cancer treatment, Luo and Lam et al. further developed pH and cis-diol dual responsive reversibly self-cross-linked telodendrimer micelles via boronic/catechol chemistry.²² Compared with chemical reactions, photoinitiated cross-linking strategy is much more attractive because of its rapid, effective, reversible, and well-controlled process that can be performed at room temperature without any additional chemicals added.^{23–25} Furthermore, the photosensitive building blocks are orthogonal to the polymer synthesis and drug loading process. The above features of photo-cross-linking make it a clean, green, and sterile process for future clinical development of the micellar nanotherapeutics.

However, the toxicity of the photochromic group and the by-products in the photoreaction have to be carefully considered. Coumarin is a natural and biocompatible substance that can undergo reversible dimerization and depolymerization under UV light of different wavelength. Zhao's group has been a pioneer in the development of reversible photo-cross-linkable coumarin-containing micelles for potential biomedical applications.^{24–26} However, the *in vivo* applications of these photosensitive polymeric micelles are usually limited by the feasibility of UV light delivery into deep tissues. Recently, the two-photon approaches via near-infrared (NIR) irradiation have been successfully applied to trigger the photosensitive micelles to release drug molecules *in vitro*, which is a step forward toward light-controllable drug release.^{27,28}

One strategy is to design a dual responsive reversible cross-linked micellar nanocarrier, which combines the clean and efficient photo-cross-linking with the responsiveness to the acidic or reducing tumor microenvironment for on-demand drug release.^{11,29} Photosensitive amphiphilic dendrimers have been developed to control the release profiles of guest molecules from the cross-linked³⁰ or non-cross-linked³¹ micelles in response to the acidic environment. Disulfide bond linkage could be applied as a built-in reversible linkage for cross-linkable nanocarrier preparation, which is normally inert to the most of polymer synthesis and chemical modifications. Disulfide bond is known to be labile upon radical treatment, such as UV irradiation, which promotes the disulfide bond exchange and allows for self-healing properties.^{32,33} However, disulfide bonds are not readily to be cleaved by UV light directly, since it largely relies on the promoted radical generation by the excess of radical initiator in the self-healing polymers.³² Very recently, photosensitive *o*-nitrobenzyl methyl ester and disulfide bonds have been introduced into the main chain³⁴ or at the block-junctions³⁵ in conventional triblock copolymers to introduce the dual responsiveness to the non-cross-linkable micelles. However, the *o*-nitrobenzyl esters linkage and its photo-degradation byproduct (e.g., nitrosobenzaldehyde) are highly suspected to be toxic in vivo.²⁵

In this study, we propose to introduce the biocompatible and photosensitive coumarin moieties into a well-defined linear-dendritic copolymer (named as telodendrimer) via a disulfide-

bond containing spacers³⁶ to prepare a series of novel dual responsive reversibly cross-linkable telodendrimers. Telodendrimers are composed of linear poly(ethylene glycol) (PEG), dendritic polylysine and specific peripheral groups, which induce the self-assembly of telodendrimers into nanocarriers for efficient *in vivo* drug delivery.^{37–39} Peptide chemistry used in telodendrimer synthesis allows for the fine-tune of the architecture and functionality of telodendrimers.^{21,22,40,41} For example, coumarin could be decorated in telodendrimer with different numbers and at different sites. On the basis of our previous work, herein, we hypothesize that introducing coumarin and a disulfide bond spacer into a telodendrimer could lead to an efficient nanocarrier with photosensitive and redox-responsive properties for efficient *in vivo* tumor targeted drug delivery.

MATERIALS AND METHODS

Materials and Equipment. Monomethyl-terminated PEG monoamine hydrochloride ($\text{MeO-PEG-NH}_2\text{-HCl}$, $M_w = 5000$ Da) was purchased from JenKem Technology. (Fmoc)Lys(Boc)-OH and (Fmoc)Lys(Fmoc)-OH were purchased from AnaSpec Inc. (San Jose, CA). The MALDI matrix α -cyano-4-hydroxycinnamic acid was analytical-grade material (Sigma-Aldrich Chemical Co.) and used as supplied. Sodium dodecyl (SDS) was purchased from Merck and used as received without further purification. PTX was purchased from AK Scientific Inc. (Mountain View, CA). 1,1'-Diocadecyl-3,3',3'-tetramethylindodicarbocyanine perchlorate (DiD) was purchased from AAT Bioquest, Inc. (Sunnyvale, CA). CellTiter 96 A_Qneous MTS reagent powder was purchased from Promega (Madison, WI, U.S.A.). Cholic acid and all other chemical reagents were purchased from Sigma-Aldrich and used as received without further purification. Dialysis membrane with a 3500 M_w cutoff was purchased from Spectrum Laboratories, Inc. Proton NMR spectra were recorded on a Bruker AVANCE 600 MHz spectrometer. Mass spectra were acquired using a Bruker REFLEX-III time-of-flight (ToF) mass spectrometer, equipped with a nitrogen laser delivering 3 ns laser pulses at 337 nm. A disulfide bond containing linker (LS) molecules was synthesized following the procedure reported in a literature.³⁶

The nomenclature of the telodendrimers followed the system used in the previous studies: For example, telodendrimer $\text{PEG}^{5k}\text{CA}_4^{\alpha}\text{LS}_4\text{Co}_4^{\epsilon}$ indicates that the molecular weight of PEG is 5 kDa and there are 4 cholic acid (CA) conjugated on the α amino groups on polylysine and 4 coumarin (Co) was conjugated on the ϵ amino groups of polylysine via linker molecules containing S-S bonds (LS).

Synthesis of Coumarin Carboxylic Acid Derivative. The coumarin-based carboxylic acid was synthesized according to literature⁴² with some modifications. The detailed synthesis procedure was as follows: 2-Bromoacetic acid (7.9 g, 56.8 mmol), 7-hydroxy-4-methylcoumarin (2.0, 11.4 mmol), potassium carbonate (15.7 g, 113.8 mmol), a trace of potassium iodide and 200 mL of ethanol were placed into a 500 mL round-bottom flask equipped with a magnetic stir and refluxed for 20 h. The mixture was then poured into 200 mL of water, followed by pH adjustment to a value of ~ 5 by addition of hydrochloric acid (5 wt %). The ethanol in the mixture was next evaporated at room temperature until a precipitate appeared. The final product was obtained at 85% yield by filtration and washed three times with water. The NMR spectrum is shown as Supporting Information Figure S1. ¹H NMR ($\text{DMSO}-d_6$, 600 MHz) δ : 7.7 (d, $J = 7.7$ Hz, 1 H, Ph-H), 6.97 (dd, $J = 8.7, 2.7$ Hz, 1 H, Ph-H), 6.93 (d, $J = 2.5$ Hz, 1 H, Ph-H), 6.22 (s, 1 H, C=CH), 4.79 (s, 3 H, CH₃).

Synthesis of Telodendrimers. The telodendrimers containing the coumarin derivative (named as $\text{PEG}^{5k}\text{Co}_8$, $\text{PEG}^{5k}\text{LS}_8\text{Co}_8$, $\text{PEG}^{5k}\text{CA}_4^{\alpha}\text{LS}_4\text{Co}_4^{\epsilon}$, and $\text{PEG}^{5k}\text{LS}_4\text{Co}_4^{\alpha}\text{CA}_4^{\epsilon}$, respectively) were synthesized using a solution-phase condensation reaction starting from MeO-PEG-NH₂-HCl (5000 Da) via stepwise peptide chemistry following our previous procedure.^{37,39} The typical synthesis of $\text{PEG}^{5k}\text{CA}_4^{\alpha}\text{LS}_4\text{Co}_4^{\epsilon}$ was as follows: (Fmoc)Lys(Fmoc)-OH (3 equiv) was coupled onto the terminal amino group on PEG using DIC and HOEt as coupling

reagents until a negative Kaiser test result was obtained to indicate completion of the coupling reaction. PEGylated molecules were precipitated by pouring reaction solution into excess amounts of cold ether, followed by centrifugation and then three times of washes with cold ether. The white powder precipitate was dried under reduced pressure and the Fmoc protecting group was removed from polymer using 20% 4-methylpiperidine solution in DMF. The subsequent coupling of (Fmoc)Lys(Fmoc)-OH and (Fmoc)Lys(Boc)-OH were carried out to generate a dendritic polylysine terminated with four Fmoc groups and four Boc groups on the peripheral of the dendron. Cholic acid NHS ester was then coupled to the Fmoc-functionalized amino groups of dendritic polylysine after removal of Fmoc group. Fmoc-protected disulfide linker was coupled to the terminal amino groups of the telodendrimers upon removal of Boc groups with 50% (v/v) trifluoroacetic acid (TFA) in dichloromethane (DCM). After removal of Fmoc groups, coumarin-based acid was finally coupled to the terminal end of dendritic polylysine. The final product was purified by dialysis for 3 days. Dialysis media was replaced by fresh water every 4 h. ¹H NMR spectra of the polymers were recorded on a Bruker 600 MHz Nuclear Magnetic Resonance Spectrometer using DMSO-d₆ as the solvent. MALDI-ToF MS spectra of telodendrimers were recorded on a Bruker REFLEX-III instrument. The hydrodynamic diameters (D_h) of the micelles and their polydispersity indexes (PDI) were determined by dynamic light scattering (DLS) on a Zetatracer Nano System. The emulsions were passed through 0.22 μm filters before DLS measurements. Each set of D_h and PDI values constituted in the average from three measurements.

Photoirradiation Procedure for Micelle Cross-Linking and De-Cross-Linking. Polymers with the alternative cholic acid (CA) and coumarin (Co) as building blocks, for example, PEG^{sk}CA₄^aLS₄Co₄^e and PEG^{sk}LS₄Co₄^aCA₄^e, self-assemble into polymer micelles in aqueous solution and the core structures could be cross-linked via photo-irradiation. As shown in Scheme 2, PEG^{sk}CA₄^aLS₄Co₄^e and PEG^{sk}LS₄Co₄^aCA₄^e are named as core non-cross-linked micelles-3 (CNM3) and core non-cross-linked micelles-4 (CNM4), respectively, before cross-linking; accordingly, the core-cross-linked micelles are named as CCM3 and CCM4, respectively. The sample was irradiated using UV light (Dymax Bluewave 200, UVA, 100 mW/cm²) or UV lamp ($\lambda = 254$ nm, 4 W) for micelle cross-linking and de-cross-linking, respectively. The cross-linking degree of micelles was characterized using UV-vis spectrometer via monitoring the percentage of the decay of the absorbance at 320 nm compared with the initial intensity.²⁶

Critical Micelle Concentration (CMC). CNM3 and CNM4 were dissolved in phosphate buffered saline (PBS). The initial micelle solution was diluted with PBS to obtain the required solutions ranging from 0.4 to 200 μg/mL. A known amount of Nile Red in MeOH was added to a series of vials. After MeOH was evaporated under vacuum, a measured amount of polymer solutions were added to each vial to obtain a final Nile Red concentration of 1 μM. The mixture solutions were left to shake overnight, in the dark, at room temperature. The fluorescence emission intensity was measured using a microplate reader (Synergy 2, BioTek Instruments, Inc.) at the wavelength of 620 nm with excitation at 543 nm. CMCs were determined at the intersection of the tangents to the two linear fitting of the curve of the fluorescence intensity as a function of the log concentration of CNM3 and CNM4.

Dynamic Light Scattering (DLS) Studies. The size and size distribution of the nanoparticles were measured using a Zetatracer (Microtrac Inc.) instrument. For the DLS particle size measurements in different organic solvents, the fluid parameters, such as refractive index and the viscosities of the solvent at two different temperatures (20 and 30 °C) were input according to the Fluid Reference Manual along with the Zetatracer instrument. The mean sizes based on the area distribution (MA) were reported. The polydispersity index (PDI) was calculated based on the formula of PDI = (SD/MA)². The micelle concentrations were kept at 5 or 10 mg/mL for DLS measurements. All measurements were performed at room temperature. To evaluate the stability of the prepared NPs, the micelle solutions were incubated at room temperature under different incubation condition, such as SDS solution, mixture solution of SDS and TCEP.

Transmission Electron Microscopy. To visualize the micelles by transmission electron microscopy (TEM), micelle solutions in dd-water were dropped onto 200 mesh copper grids, coated with carbon film for 1 min and then the droplet was removed by filter paper. Subsequently, a drop of RuO₄ solution was dropped immediately onto the copper grids for 1 min to stain the sample grids. Then staining solution was removed completely via filter paper and air-dried before observed under a JEOL JEM-2100 HR instrument operating at a voltage of 200 kV.

Preparation and Characterization of Drug-Loaded Micelles. PTX was loaded into telodendrimer micelles via a dry-down (evaporation) method as described previously.^{37,39} Briefly, 10 mg of telodendrimer along with 1 mg of paclitaxel were first dissolved in CHCl₃ and evaporated using a rotavaporator to obtain a dry, homogeneous polymer film. The film was reconstituted in 1 mL of PBS, followed by sonication to disperse micelles. No precipitation was observed with the monodispersed particle size from 15 to 30 nm measured via DLS, which indicated the complete drug loading. To track the biodistribution of nanoparticles, hydrophobic NIRF dye DiD was encapsulated with PTX into the micelles using the same method as described above. The particle sizes of the micelle solution were measured via a DLS particle sizer. Finally, the micelle formulation was filtered with 0.22 μm filter to sterilize the sample. The drug loading capacity (DLC) and drug loading efficiency (DLE) were defined by the following equations:

$$\text{DLC (\%)} = \frac{\text{weight of loaded drug}}{\text{weight of drug-loaded NPs}} \times 100\%$$

$$\text{DLE (\%)} = \frac{\text{weight of loaded drug}}{\text{weight of drug in feed}} \times 100\%$$

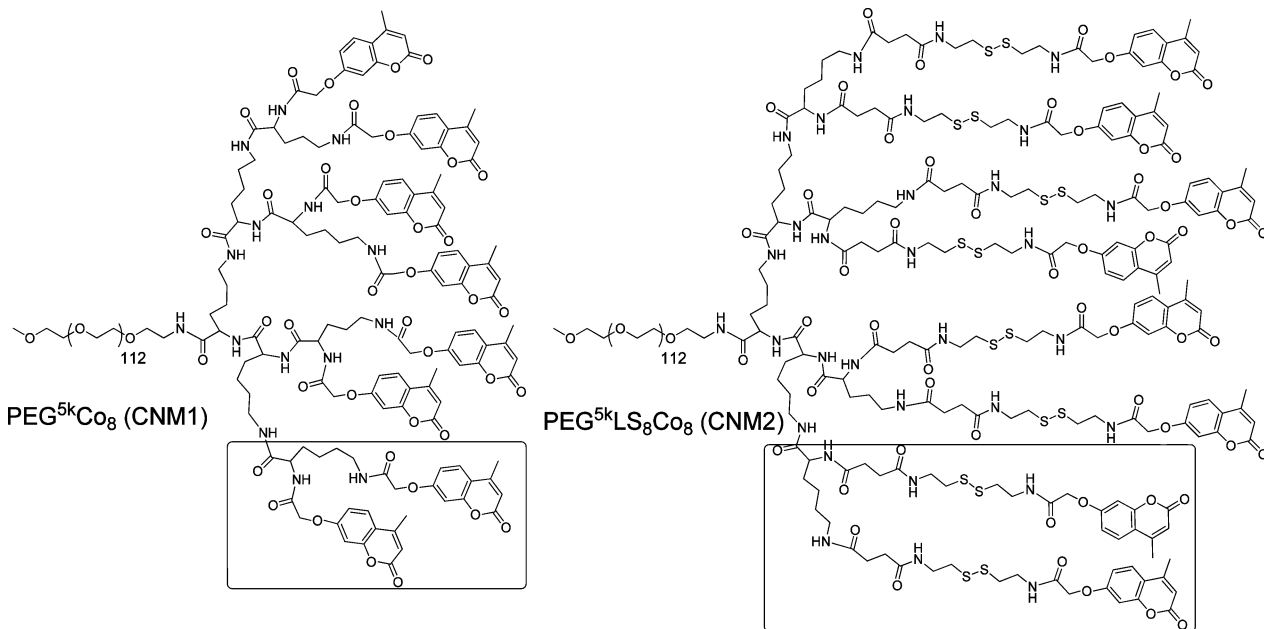
In Vitro Release of PTX. PTX-loaded non-cross-linked and cross-linked micelles with 5:0.5 ratio of the polymer to PTX were prepared in PBS. Aliquots of PTX-loaded micellar solution were put into dialysis cartridges with a molecular weight cutoff of approximately 3500 Da. The cartridges were dialyzed against dd-water at room temperature, which was stirred gently at a speed of 150 rpm. The concentration of PTX remaining in the dialysis cartridge at various time points was measured by HPLC. Three replicate dialyses were conducted.

Hemolytic Assays. One milliliter of fresh blood from healthy human volunteers was collected into 5 mL of PBS solution in the presence of 20 mM EDTA. Red blood cells (RBCs) were then separated by centrifugation at 1000 × g for 10 min. The RBCs were washed three times with 10 mL of PBS and resuspended in 20 mL of PBS. Diluted RBC suspension (200 μL) was mixed with polymers at serial concentrations (10, 100, 500, and 1000 μg/mL) by gentle vortex and incubated at 37 °C. After 0.5 h, 4 h, and overnight, the mixtures were centrifuged at 1000 × g for 5 min. The supernatant free of hemoglobin was determined by measuring the absorbance at 540 nm using a UV-vis spectrometer. Incubations of RBCs with Triton-100 (2%) and PBS were used as the positive and negative controls, respectively. The percent hemolysis of RBCs was calculated using the following formula:

$$\begin{aligned} \text{RBC hemolysis} &= 100\% \times (\text{OD}_{\text{sample}} - \text{OD}_{\text{PBS}}) \\ &/(\text{OD}_{\text{triton}} - \text{OD}_{\text{PBS}}) \end{aligned}$$

Cell Culture and MTS Assays. The ovarian cancer cell line SKOV-3 and the colon cancer cell line HT-29 were purchased from American Type Culture Collection (ATCC, Manassas, VA, U.S.A.). All cells were cultured in McCoy's 5A medium supplemented with 10% fetal bovine serum (FBS), 100 U/mL penicillin G, and 100 μg/mL streptomycin at 37 °C using a humidified 5% CO₂ incubator. SKOV-3 cells were seeded in 96-well plates at a density of 4000 cells/well 24 h prior to the treatment. Empty micelles and various formulations of PTX with different dilutions were added to the plate and then incubated in a humidified 37 °C, 5% CO₂ incubator. After a 72 h incubation, a mixture solution composed of CellTiter 96 AQ_{neous} MTS, and an electron coupling reagent, PMS, was added to each well according to the

Scheme 1. Chemical Structures of Telodendrimers with Coumarin As Periphery Groups with and without Spacers Containing Disulfide Bond



manufacturer's instructions. The cell viability was determined by measuring absorbance at 490 nm using a microplate reader (BioTek Synergy 2). Untreated cells served as the control. Results were shown as the average cell viability $[(OD_{treat} - OD_{blank})/(OD_{control} - OD_{blank}) \times 100\%]$ of triplicate wells. The cells were also treated with blank non-cross-linked and cross-linked micelles with different dilutions and incubated for a total of 72 h to evaluate polymer-related toxicity.

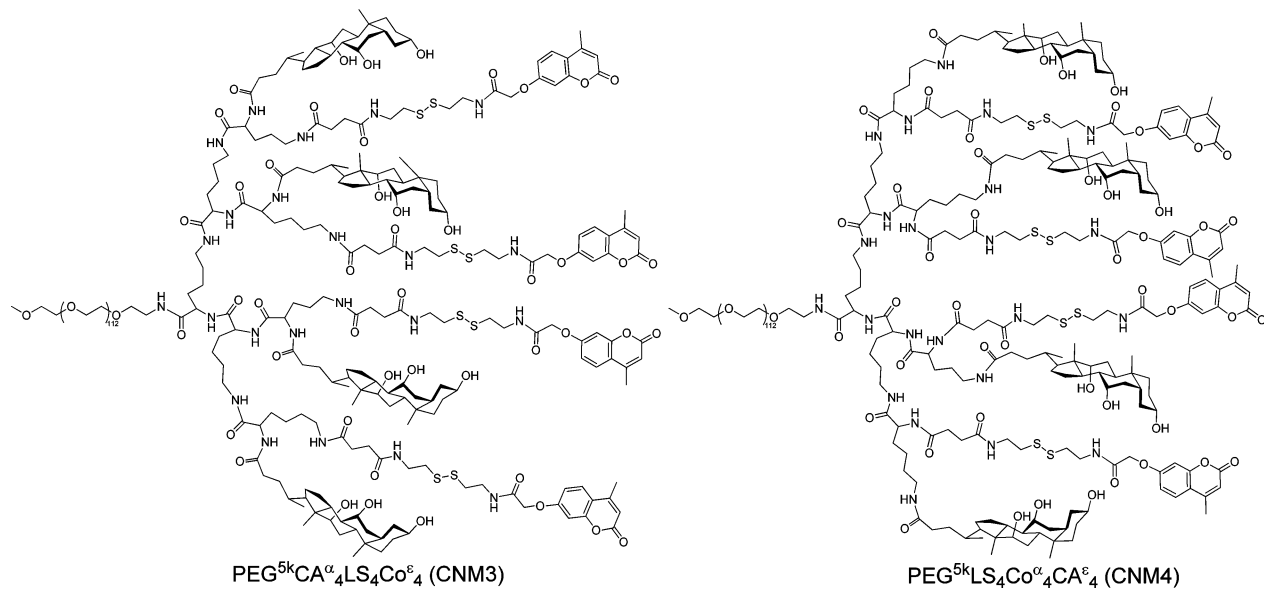
Animal Xenograft Models and the Fluorescence Animal Imaging. Female athymic nude mice (Nu/Nu strain), 5–6 weeks of age, were purchased from Harlan (Livermore, CA, U.S.A.). All animals were kept under pathogen-free conditions according to AAALAC (Association for Assessment and Accreditation of Laboratory Animal Care) guidelines and were allowed to acclimatize for at least 4 days prior to any experiments. All animal experiments were performed in compliance with institutional guidelines and according to protocol approved by the Committee for the Humane Use of Animals of State University of New York Upstate Medical University. A subcutaneous colon cancer xenograft mouse model was established by injecting 1×10^7 HT-29 cancer cells in a $100 \mu\text{L}$ of mixture of PBS and Matrigel (1:1 v/v) subcutaneously at the right flank in female nude mice.

Hydrophobic NIRF dye (DiD) was encapsulated together with PTX into the micelles using the same method as described above. The DiD-PTX coloaded non-cross-linked micelles and cross-linked micelle formulation were filtered with a $0.22 \mu\text{m}$ filter to sterilize the sample. About 3 weeks after tumor inoculation, nude mice with subcutaneous tumors of approximate 8–10 mm ($\sim 300\text{--}500 \text{ mm}^3$) in diameter were subjected to in vivo NIRF optical imaging. DiD fluorescently labeled non-cross-linked/cross-linked micelles together with paclitaxel and free DiD in $100 \mu\text{L}$ of PBS were injected into HT-29 or SKOV-3 tumor xenografts bearing nude mice via the tail vein, respectively. Mice were anesthetized and optically imaged at different time points (1, 2, 4, 8, 24, 48 and 72 h) using an IVIS 200 (PerkinElmer) with the excitation at 625 nm and the emission at 700 nm. At the end of the experiment, the animals were sacrificed and all the major organs and tumors were excised for ex vivo imaging. The accumulated fluorescence intensities were determined by Living Image software (Caliper Life Sciences) using operator-defined regions of interest (ROI) measurements.

Statistical Analysis. The level of significance in all statistical analyses was set at a probability of $P < 0.05$. Data are presented as the standard error of the means (SEM). Statistical analysis was performed by Student's *t* test for comparison of two groups.

RESULTS AND DISCUSSION

Coumarin (Co) is a photosensitive molecule which undergoes dimerization and dissociation upon UV irradiation at different wavelengths, for example, UV $> 310 \text{ nm}$ or UV $< 280 \text{ nm}$, respectively.^{25,43} 4-Methylcoumarin has been reported to be more reactive than coumarin in response to photo irradiation.⁴⁴ In this study, 4-methylcoumarin was therefore applied for the development of reversibly photo-cross-linkable micelles via a derivative of 7-(carboxymethoxy)-4-methylcoumarin (Supporting Information Scheme S-1 and Figure S1). Luo and Lam and their colleagues have developed a telodendrimer system, which is a linear-dendritic block copolymer system composed of PEG and dendritic oligo-cholic acid (e.g., PEG^{5k}CA₈). Telodendrimer system has a well-defined structure prepared via stepwise peptide chemistry.^{37,39} Preparation of a photoresponsive reversibly cross-linkable telodendrimer PEG^{5k}Co₈ by replacing cholic acid with coumarin, as shown in Scheme 1, was easily achieved. In addition, we have also synthesized a telodendrimer PEG^{5k}LS₈Co₈ containing linkers with disulfide bonds (LS) prior to coumarin conjugations (Scheme 1). The structures of these two telodendrimers have been characterized via proton NMR, where eight coumarin molecules were detected relative to the methyl group proton signal on MeO-PEG (Supporting Information Figures S2 and 3). UV irradiation ($>310 \text{ nm}$) is efficient, convenient and clean for micelle cross-linking in vitro after drug loading. The preserved disulfide bond spacer molecule is able to respond to the reducing reagents, such as high concentration glutathione ($\sim 10 \text{ mM}$) within the tumor intracellular microenvironment,^{45,46} where photo de-cross-linking is not easily achievable because of poor penetration and cytotoxicity of UV light. Furthermore, the elongated distance for two adjacent coumarin molecules via S-S spacers could reduce the chance of intramolecular dimerization of coumarin moieties, which has no contribution to the integrity of micelles. To test this hypothesis, we have synthesized small molecular coumarin dimers (Supporting Information Scheme S-1) with or without S-S linker molecules via solid phase

Scheme 2. Structures of Two Coumarin-Containing Telodendrimers ($\text{PEG}^{\text{sk}}\text{CA}^{\alpha_4}\text{LS}_4\text{Co}^{\varepsilon_4}$ and $\text{PEG}^{\text{sk}}\text{LS}_4\text{Co}^{\alpha_4}\text{CA}^{\varepsilon_4}$)^a

^aCNM refers to the core non-cross-linked micelles; CCM refers to the core cross-linked micelles after photo-irradiation.

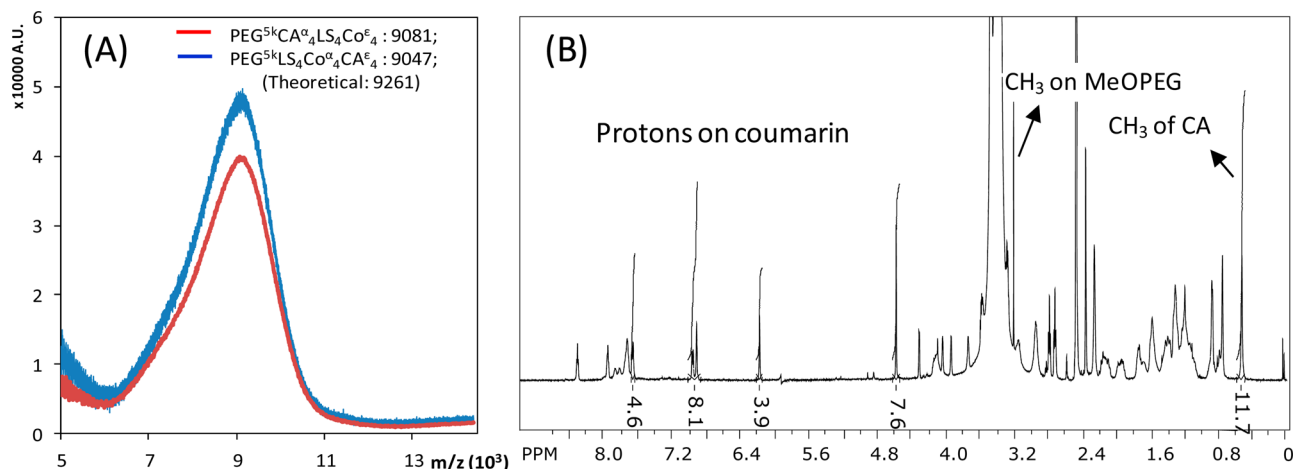


Figure 1. (A) MALDI-TOF mass spectra of $\text{PEG}^{\text{sk}}\text{CA}^{\alpha_4}\text{LS}_4\text{Co}^{\varepsilon_4}$ and $\text{PEG}^{\text{sk}}\text{LS}_4\text{Co}^{\alpha_4}\text{CA}^{\varepsilon_4}$ and (B) the ^1H NMR spectrum of $\text{PEG}^{\text{sk}}\text{CA}^{\alpha_4}\text{LS}_4\text{Co}^{\varepsilon_4}$. The proton NMR spectrum of $\text{PEG}^{\text{sk}}\text{LS}_4\text{Co}^{\alpha_4}\text{CA}^{\varepsilon_4}$ is shown in Supporting Information Figure S6.

synthesis, which are the subunits of telodendrimers as marked in Scheme 1. The photo-cross-linking studies of these dimers in DMSO revealed a significant decrease (~3-fold) in dimerization rate for coumarin dimers with S–S linkages (Supporting Information Figure S4) at the same concentration to the coumarin dimers without S–S linkages. In addition, no dimerization could be observed for coumarin monomers under the same conditions. Further, the coumarin dimerization in telodendrimer micelles with S–S spacers is significantly accelerated, which may due to the increased local concentration of coumarin and increases the opportunity of intermolecular dimerization.

$\text{PEG}^{\text{sk}}\text{Co}_8$ self-assembles into micelles in aqueous conditions with a homogeneous particle size of 24 ± 6 nm, termed as the core non-cross-linked micelle-1 (CNM1). $\text{PEG}^{\text{sk}}\text{LS}_8\text{Co}_8$ could also form homogeneous micelles with bigger particle sizes of 43 ± 13 nm due to the introduction of the hydrophobic S–S linkers. However, these two micelles performed poorly in loading anticancer drugs, such as paclitaxel (PTX), with

heterogeneous particle sizes and low loading efficiency (24% at 10:1 polymer/drug ratio) (Supporting Information Figure S5). Heterogeneous size distribution and precipitation was observed right after drug loading or after storage overnight. It was expected that the small aromatic structure of coumarin could not efficiently hold the drug molecules and the balance of the hydrophobic and hydrophilic components in such micelle systems could be easily altered by the addition of hydrophobic drug molecules. Our previous studies revealed that the unique facial amphiphilic structure of cholic acid (CA) in telodendrimer plays an important role in stabilizing this micelle system, compared with other pure hydrophobic molecules with similar structures, such as cholesterol, lithocholic acid, etc.³⁷ It is believed that CA could reduce the surface tension between the hydrophobic core and the aqueous PEG layer in the micelles via adapting the favorable molecular orientation: for example, hydrophilic hydroxyl-enriched surface facing toward the aqueous phase and hydrophobic layer facing inside the micelle core. Therefore, CA was kept as a co-core forming building

Table 1. Characterization and Drug Loading Properties of Telodendrimers

	formula (via NMR)	M_w		PTX-loaded micelles			after cross-linking	
		MS	theoretical	size (nm)	DLC (%) ^a	DLE (%) ^b	size (nm)	DC (%) ^c
CNM3	PEG ^{sk} CA _{3.8} LS ₄ Co _{4.1}	9081	9261	17 ± 4	>30	98	16 ± 4	78
CNM4	PEG ^{sk} Co _{4.0} LS ₄ CA _{4.3}	9047	9261	20 ± 5	>20	99	19 ± 5	81

^aDrug loading content. ^bDrug loading efficiency. ^cDegree of cross-linking under a UVA >310 nm at 100 mW/cm².

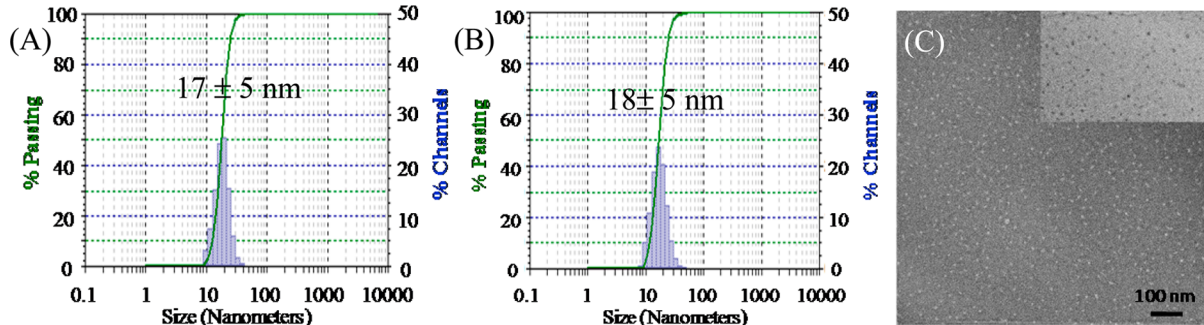


Figure 2. DLS particle sizes of micelles formed by PEG^{sk}CA₄LS₄Co₄: (A) before photo-cross-linking CNM3 and (B) after photo-cross-linking CCM3. (C) Normal TEM image of CCM3 with negative staining and the right-up corner was black-white phase inverted.

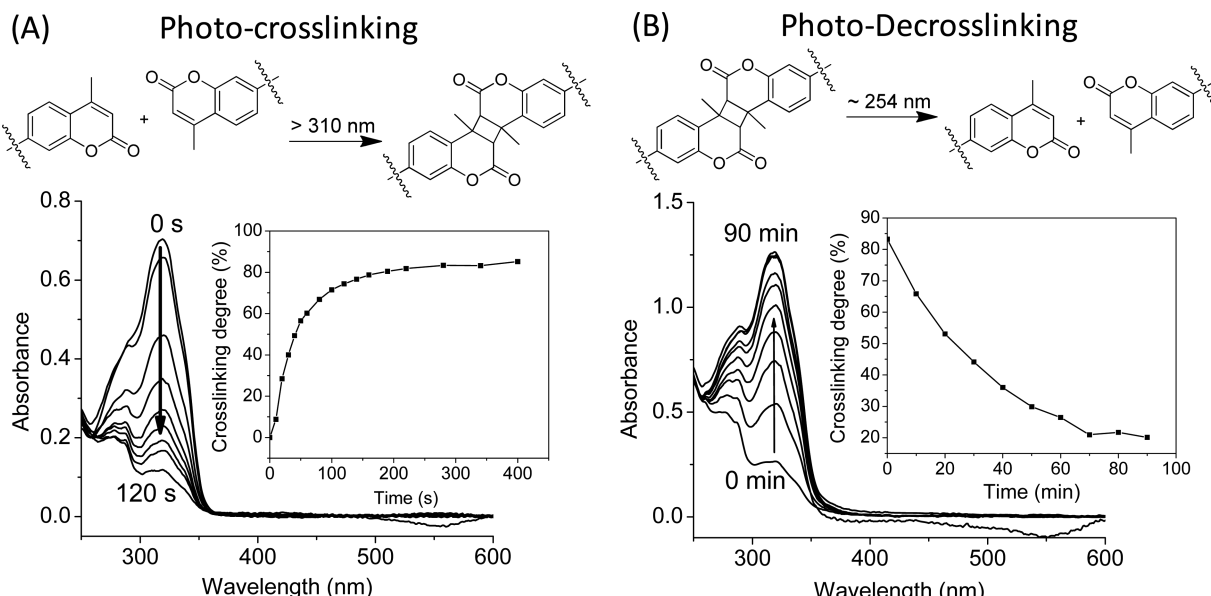


Figure 3. UV-vis spectra of a micellar solution of CNM3 formed from PEG^{sk}CA₄LS₄Co₄ under UV irradiation, sequentially, at different wavelength: (A) under UV irradiation at $\lambda > 310$ nm, the inset showing the increase in coumarin dimerization degree (micelle cross-linking) over seconds; (B) under UV irradiation at ~ 254 nm, the inset showing the decrease in the cross-linking degree over minutes.

block with coumarin in the development of photosensitive telodendrimers.

We further prepared another two telodendrimers with alternating peripheries of cholic acid and coumarin onto the α and ϵ position of lysine, respectively, as shown in Scheme 2. The coumarin molecule was introduced onto the telodendrimer via a S-S spacer (shown in Supporting Information Scheme S-2 and S-3) to preserve the reversibility in response to the tumor intracellular reducing microenvironment. These telodendrimers, for example, PEG^{sk}CA₄LS₄Co₄ and PEG^{sk}LS₄Co₄CA₄ self-assemble into micelles CNM3 and CNM4 with monodispersed particle sizes. Their structures were confirmed by ¹H NMR and MALDI-TOF MS. As shown in the ¹H NMR spectrum of Figure 1, characteristic peaks at 6.18 and 0.57 ppm were attributed to the single vinyl proton on coumarin and C18 methyl group of

cholic acid, respectively. The integrations of these two peaks were calculated to be very close to 4 (4 C=CH-) and 12 (4 CH₃) relative to the methyl protons (CH₃) of MeO-PEG (Table 1), indicating four coumarin molecules and four cholic acids were precisely conjugated onto telodendrimers as originally designed. Furthermore, the molecular weights of both polymers obtained via MALDI-TOF MS were very close to the theoretical values, suggesting well-defined structures of telodendrimers via peptide chemistry. It should be noted that the known underestimation of the high molecular weight polymers in MALDI-TOF analysis might attribute to the difference between the observed and theoretical molecular weight. The polymer characterization data were summarized in Table 1.

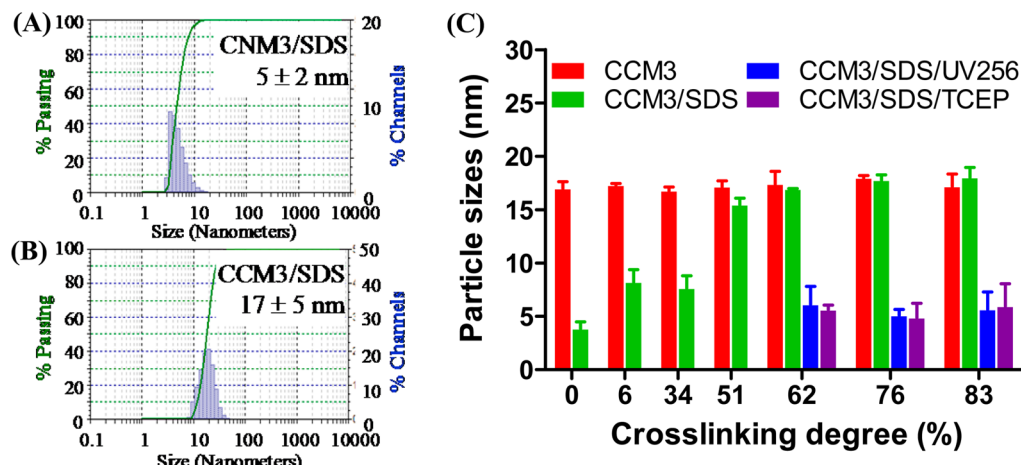


Figure 4. (A) DLS particle size of non-cross-linked micelles CNM3 shrunk to 5 nm in the present of SDS. (B) DLS particle size of core-cross-linked micelles CCM3 maintained at 17 nm in the present of SDS. (C) Systematic evaluation of the enhanced stability of CCM3 micelles with different cross-linking degree in the absence/presence of SDS and the additional treatment to de-cross-linking micelles, for example, UV254 irradiation and reducing reagent of TCEP. The final concentrations of polymer and SDS were 1 and 2.5 mg/mL, respectively. The data were presented as mean with SD of three measurements.

CNM3 and CNM4 both could form stable micelles with monodispersed particle sizes of 17 ± 5 nm (Figure 2) and 14 ± 3 nm (Supporting Information Figure S7), respectively. The PEG^{sk}CA^aLS₄Co^e with CA on the α -amino of lysine, has better spatial segregation of CA and Co moieties than PEG^{sk}LS₄Co^aCA^e, as shown in Scheme 2. Such structure may contribute to the favorable photo-cross-linking profile and better micelle stability and drug loading capacity, due to the minimized interfacial energy by the amphiphilic CA layer located between the PEG layer and the more hydrophobic coumarin-enriched core structure. CNM3 indeed exhibited higher PTX loading capacity (Table 1) and better reproducibility than CNM4. The critical micelle concentration (CMC) of CNM3 and CNM4 was detected to be about 15 and 17 μ g/mL, respectively, using Nile-red as fluorescent probe (Supporting Information Figure S8). The particle size of CNM3 was determined by dynamic light scattering (DLS) to be around 17 ± 5 nm (Figure 2A), which remained almost unchanged after photoirradiation under UV >310 nm (Figure 2B). Further, TEM images of the cross-linked micelles CCM3 from PEG^{sk}CA^aLS₄Co^e revealed the presence of presumably spherical micelles of around 15–20 nm in diameter, which was consistent with the DLS measurement.

To study the photo-cross-linking and reversible de-cross-linking process of photosensitive telodendrimer micelles, the characteristic absorption of monomer coumarin at 320 nm was monitored via UV-vis spectrometer, while CNM3 micelle solution was irradiated sequentially under UV light at different wavelengths (Figure 3). When the micellar solution (4 mg/mL) was exposed to UV light at $\lambda > 310$ nm (100 mW/cm² from a UV-vis spot curing system), the absorbance of coumarin moieties at 320 nm decreased quickly within 2 min, indicating the occurrence of coumarin dimerization and micelle cross-linking within the core structure. The inset in Figure 3A of CNM3 displayed very rapid cross-linking kinetics, where dimerization degree reaches up to 60% within 1 min of irradiation at UV $\lambda > 310$ nm. Furthermore, cross-linking degree could be precisely controlled by varying irradiation time or light energy. When the core cross-linked micellar (CCM3) solution was treated under a UV lamp ($\lambda = 254$ nm, 4 W), the reversible process, i.e. photo induced cleavage of coumarin dimers, took place as indicated by the recovery of the absorbance at 320 nm

as shown in Figure 3B. The decrease in the dimerization degree is also shown in the inset of Figure 3B. Although the photocleavage of coumarin dimers appeared to be incomplete due to the photo saturation, a reversible de-cross-linking of micelles could be achieved to a certain degree (20% cross-linking remained after 2 h irradiation). Interestingly, it was observed that the cross-linking and de-cross-linking process could be efficiently repeated for three recycles with only slightly decrease in the reaction rate (Supporting Information Figure S9). Although this repeatability may not be applicable for in vivo application, it allows for the precise control of cross-linking degree via UV illumination. The CNM4 has similar photo-cross-linking and de-cross-linking profiles with CNM3 (Supporting Information Figure S10).

Sodium dodecyl sulfate (SDS) is able to efficiently disassemble polymeric micelles via charge repulsion after insertion into the polymer micelle structure, which is often used to challenge the stability of the cross-linked micelles.^{20–22} As shown in Figure 4A, the stability of non-cross-linked CNM3 was poor and the particle size was reduced from 17 to 5 nm upon the addition of SDS. However, the cross-linked micelles of CCM with 83% cross-linking degree remained stable at 18 nm particle size in the presence of 2.5 mg/mL SDS (Figure 4B). The experimental results indicated the successful cross-linking of the micelles and high stability. Furthermore, the stability of micelles with different cross-linking degree was systematically investigated under the different condition by DLS. Disulfide bonds can be selectively cleaved under mild condition using various reductive reagents, such as DTT, glutathione, TCEP, etc., in addition to the photocleavage of coumarin dimer for micelle de-cross-linking. As shown in Figure 4C, micelles with cross-linking degree in the range of 0–80% were prepared for the stability measurement. With increases in cross-linking degree, the stability of micelles increases in the presence of SDS. When cross-linking degree is higher than 50%, no significant size reduction for CCM3 was observed in the presence of SDS. Instead, a slight size increase was observed for the CCM3 micelle with 61% cross-linking degree, which may be due to micelle swelling from SDS insertion. Next, to induce micelle de-cross-linking, reductive TCEP (10 mM), and UV radiation at 254 nm were applied, respectively, to the CCM3 with cross-

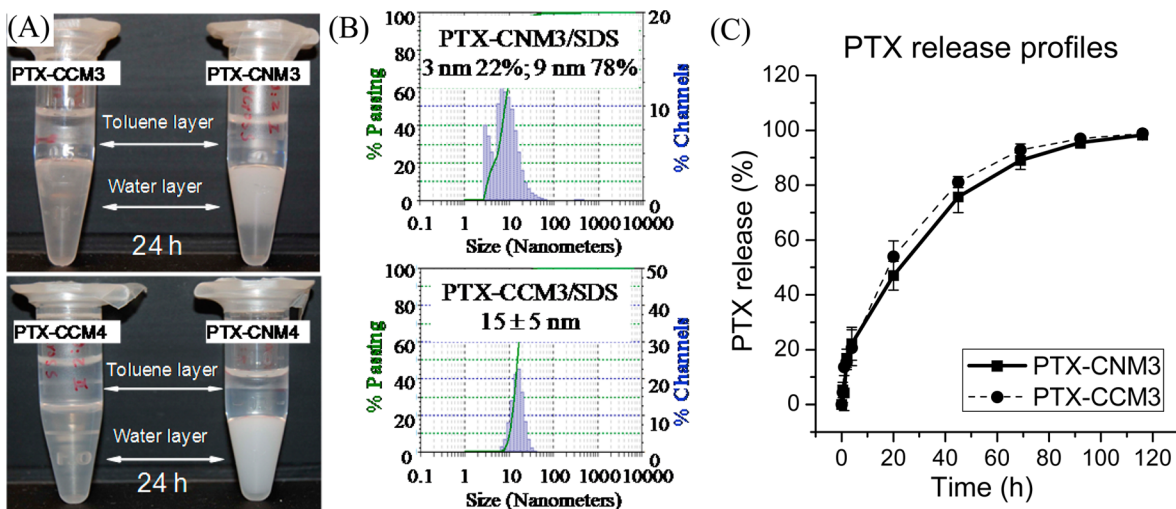


Figure 5. (A) Stability of the PTX loaded CNM3 and CCM3 solution against incubation with toluene for 24 h (drug/polymer = 1/10 mg/mL; cross-linking degree = 56%). (B) Size stability of the non-cross-linked PTX-CNM3 and cross-linked PTX-CCM3 in the presence of SDS (polymer/SDS = 1/2.5 mg/mL, respectively). (C) PTX-release profiles from the non-cross-linked CNM3 and the photo-cross-linked CCM3.

linking degree higher than 50%. As shown in Figure 4C, both TCEP and UV 254 nm radiation could efficiently de-cross-link micelles with even 80% cross-linking degree, which then was disassembled by SDS. It was noticed that TCEP could break down micelles more efficiently in the presence of SDS as opposed to the UV radiation at 254 nm.

Paclitaxel is a very effective antineoplastic drug used clinically to treat a broad spectrum of cancers. PTX was successfully loaded into non-cross-linked micelles with high efficiency (98–99% drug loading efficiency via HPLC measurement) for both CNM3 and CNM4. The particle sizes of PTX loaded CNM3 were measured to be 17 nm as shown in Table 1, which was only slightly increased compared to the empty micelles (16 nm). However, PTX-CNM4 had a particle size of 20 nm with a significant increase in size when compared with the empty CNM4 (14 nm) (Supporting Information Figure S11). It is also noticed that CNM3 could encapsulate PTX with higher content (~30%) and better reproducibility as opposed to CNM4 (~20%). This may be due to the difference in the structural geometry between these two telodendrimers as discussed above. After photo-cross-linking, PTX-loaded CCM3 and CCM4 with 78–81% cross-linking degree had only slight shrink in size, while maintaining the same drug loading contents and narrow particle size distribution.

It is expected that the cross-linking of micelles could stabilize drug encapsulation within the micelle nanocarrier by limiting the drug diffusion and maintaining the integrity of micelle nanoparticles. In our previous study, we observed that the telodendrimer could form core-inversed micelles (CIMs) in some apolar solvents, such as toluene and ethyl acetate.³⁸ CIMs could be efficiently extracted into aqueous solution because of the hydrogen bonding and dominant partition of PEG in water as opposed to an apolar solvent. Therefore, it will be interesting to study the properties of micelles at the water–toluene interface, which should be occupied by the facial amphiphilic CA and hydrophobic coumarin moieties. This may lead to the instability of micelles and the leakage of the payload drugs from the nanocarrier. As shown in Figure 5A, the aqueous solutions of PTX loaded micelles before and after photo-cross-linking, for example, CNM3, CNM4, CCM3, and CCM4 (about 56% cross-linking degree), were incubated standstill against toluene over

24 h. As expected, the aqueous solution of non-cross-linked PTX-CNM3 and PTX-CNM4 solutions became opaque from the aqueous–oil interface. In contrast, the cross-linked PTX-CCM3 micelle solution remained clear over time, with only a thin layer of opaqueness observed at the interface. The formation of an emulsion took place at the water–oil interface, where free amphiphiles accumulate and micelles dissociate. Subsequently, the engulfment of toluene droplets, stabilized via the single layer of telodendrimer, into aqueous solution could be induced by Brownian motion or mechanical vibrations. For the non-cross-linked micelles, PTX leaked out at the aqueous–oil interface from the destabilized micelles, which would be either diffused into toluene layer or precipitated out from the aqueous solution. Indeed, PTX precipitation was collected via centrifugation at the bottom of the aqueous layer and confirmed by HPLC analysis. The PTX loaded CNM4 was observed to be less stable than PTX-CNM3, which showed the emulsion formation even as earlier as 2 h after incubation, whereas the PTX-CNM3 solution was still clear (Supporting Information Figure S12). The turbidities of these two aqueous solutions were measured at 2 h via UV–vis absorbance at 660 nm and found to be 1:4 for PTX-CNM3 to PTX-CNM4. For the cross-linked micelles, nanoparticles are stable against the interruption at the water–oil interface. However, PTX could be extracted into toluene layer after release from nanocarriers. The ratio of the PTX concentrations in aqueous phase and in toluene layers after the incubation of cross-linked PTX-micelle solutions against toluene for 24 h were analyzed via HPLC to be 1:2 and 1:3 for CCM3 and CCM4, respectively, which indicates the better affinity of PTX within CCM3 than CCM4. This novel method allows us to evaluate the efficiency of the nanocarrier cross-linking in stabilizing micelles and the payloads.

In addition, the PTX-loaded CNM3 and CCM3 were incubated with SDS and the particle sizes of the PTX-CNM3 shrunk and become heterogeneous (Figure 5B), whereas cross-linked PTX-CCM3 micelles (56% cross-linking degree) retained the particle sizes around 15 nm. This also indicated an improved stability for the PTX-loaded nanocarrier via photo-cross-linking of coumarin moieties. In addition, it was demonstrated that the PTX release from CNM3 was faster in the presence of SDS than from CCM3 (Supporting Information Figure S13).

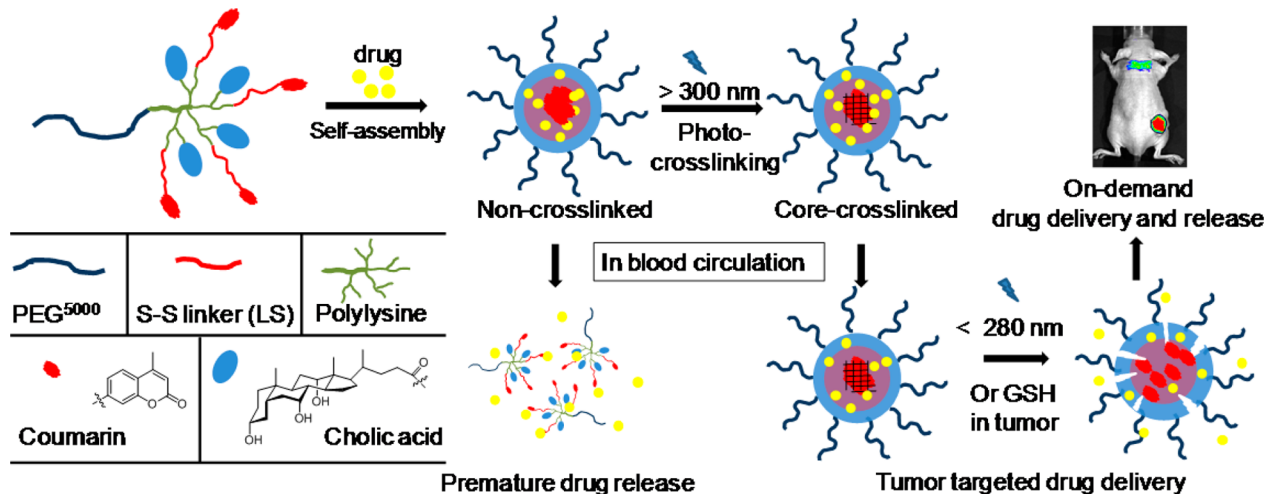


Figure 6. Illustration of the cross-linking and de-cross-linking process of the coumarin containing photosensitive phase-segregated micelle nanocarriers.

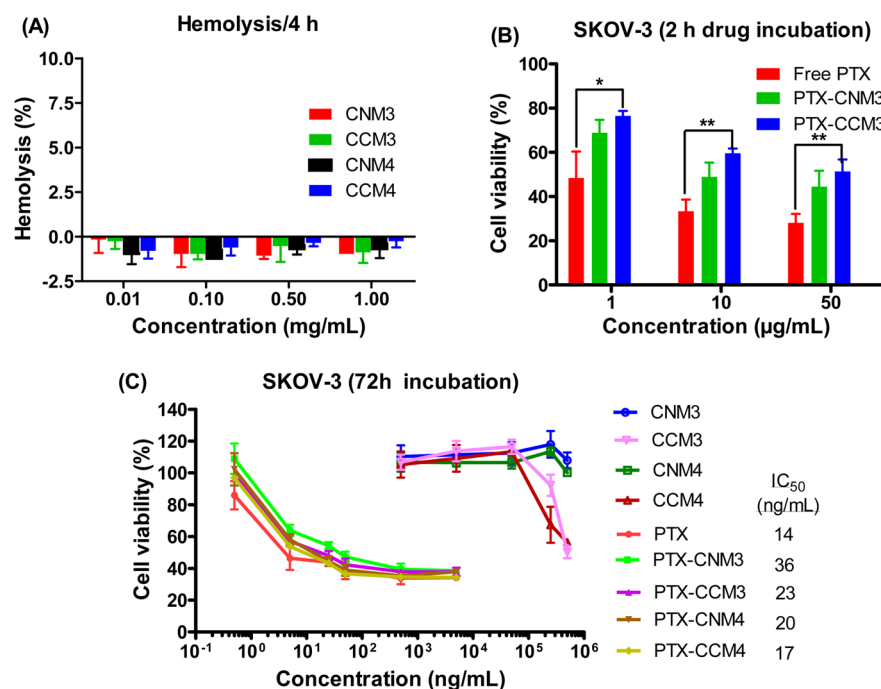


Figure 7. (A) Hemolytic property of the cross-linked and non-cross-linked micelles. (B) Cytotoxicity of PTX loaded CNM3 and CCM3 in comparison with free PTX on SKOV-3 ovarian cancer cells after 2 h drug exposure and 72 h continuous drug incubation. (C) Cell viability assays on the SKOV-3 cells after 72 h continuous drug incubation for free polymer and PTX-loaded cross-linked and non-cross-linked micelles (triplicate data were presented as mean \pm SD; * p < 0.05; ** p < 0.01).

Furthermore, we evaluated the effects of the micelle cross-linking on the in vitro PTX drug release in biological relevant environment, for example, 37 °C in PBS. PTX-NCM and PTX-CCM solutions in PBS were placed in a dialysis bag with MWCO of 3500 Da and dialyzed against the frequently refreshed 4 L of PBS. PTX release profiles were studied via HPLC analysis of drug concentration within the dialysis bag over time. As shown in Figure 5C, no burst release was observed and about 50% and 100% of PTX was released by 24 and 120 h, respectively, for both CNM and CCM. Surprisingly, no significant difference between the cross-linked CCM and the non-cross-linked CNM on PTX release was observed in the repeated experiments via the dialysis method, where the static diffusion of PTX dominants the drug release rate. One possible

reason is that the drug molecules may be trapped between the amphiphilic CA-enriched layer and the coumarin-enriched cross-linked core interior of the micelle (as shown in Figure 6). Therefore, the core-cross-linking of micelles has less impact on the PTX diffusion rate. Although it is hard to prove this hypothesis, however, it is coincident with the preferred PTX encapsulation in CA-enriched PEG^{sk}CA₈ micelles (>35% PTX content)^{37,39} as opposed to the poor loading of PTX in the Coumarin-containing PEG^{sk}Co₈ micelles as described earlier (Supporting Information Figure S5).

The monomeric aromatic coumarin may have a tendency to form $\pi-\pi$ stacking within the core of micelles, which may lead to phase separation from the cholic acid and PTX, especially before photo-cross-linking. It might also be the reason for the

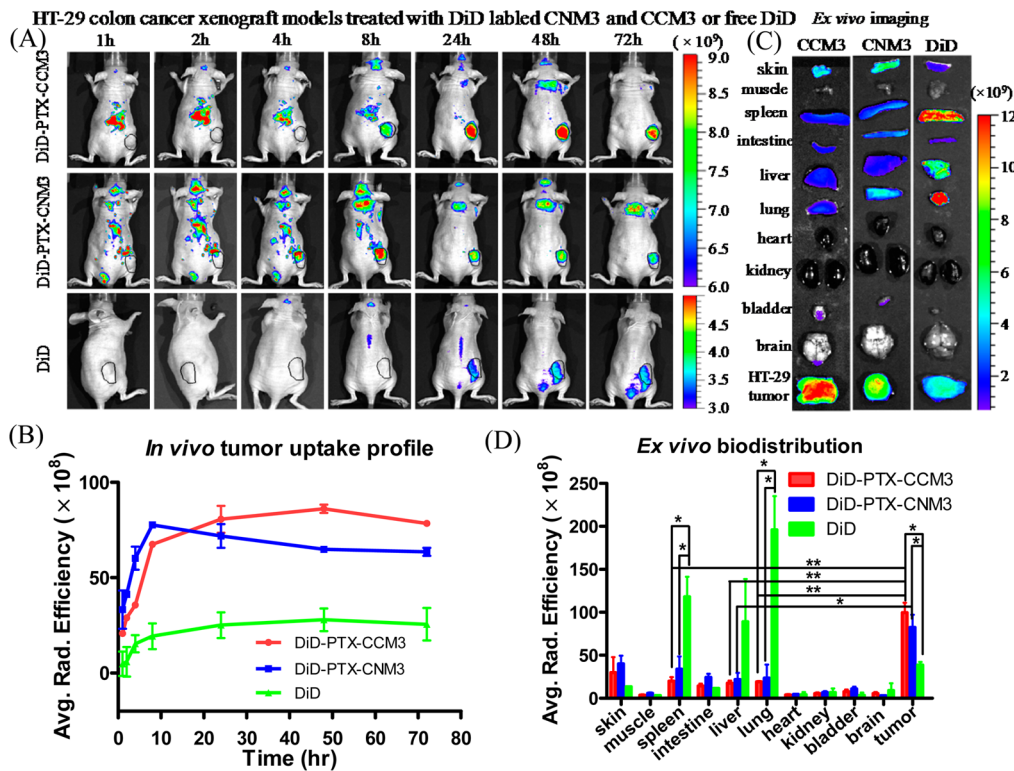


Figure 8. (A) In vivo NIR fluorescence imaging of the animals bearing HT-29 colon cancer xenografts after treated with DiD-PTX coloaded micelles and free DiD through tail vein injection. The nonspecific signals on skin mostly are colocalized with the scarring tissue by bite for male animals. (B) In vivo tumor uptake profiles of the fluorescent signals after tail vein injection of the free DiD and cross-linked or non-cross-linked micelles coloaded with DiD and PTX (average of two animals). (C) Ex vivo images of the tumor and organs after 72 h post injection. (D) Ex vivo biodistribution of the fluorescent signals in different organs and tumors (average of two animals, * $p < 0.05$; ** $p < 0.01$).

accelerated photodimerization of coumarin after conjugated onto telodendrimer and aggregated into micelles (60% cross-linking in 60 s), compared with the small molecular coumarin dimer **2** with S-S linkages (20% cross-linking in 60 s, Supporting Information Figure S4). More importantly, the dimerization of coumarin within the telodendrimer micelles could increase the integrity of nanoparticles in the biological environment, which provides opportunity for nanoparticles to target tumor via passive targeting effects through the tumor leaky blood vessels. In contrast, the extreme dilution and the interaction with the hydrophobic proteins and cytoplasm membrane may dissociate the non-cross-linked micelles instantly, leading to the premature drug release and fast clearance from blood circulation (as illustrated in Figure 6). Therefore, it is still expected that the cross-linked micelles CCM3 may deliver more drug molecules to tumor site than CNM3 via the known EPR effects^{7,8} of nanoparticles with the improved integrity.

The in vitro hemolytic properties of the non-cross-linked and cross-linked micelles has been tested to be negligible up to 1 mg/mL of micelle concentration for 4 h incubation at 37 °C as shown in Figure 7A. The empty non-cross-linked micelles showed noncytotoxicity up to 0.5 mg/mL. While moderate cell growth inhibition were observed for the photo-cross-linked micelles at high concentrations 0.25–0.5 mg/mL, which may be due to the free radical and active oxygen species caused by UV irradiation. (Figure 7C). The reduced cytotoxicities of PTX-loaded micelles, especially for CCM3 formulation, were observed compared with free PTX after 2 h drug exposure in cell culture (Figure 7B). This is due to the enhanced

nanoparticle stability and the slow release of drug from micelle nanocarriers during cell culture, which may indicate the reduced toxic side effects to normal organs during systemic administration. Further, after continuous 72 h drug incubation, slightly decreased cytotoxicity, however not significant, for the nanoformulations were observed relative to the free PTX as shown in Figure 7C.

Given the better drug loading capacity and stability of CNM3 compared with CNM4 micelles, we would focus the in vivo studies on CNM3 and CCM3. DiD is a hydrophobic near-infrared fluorescence cyanine dye, which could be stably entrapped within nanocarrier to represent the distribution of the nanocarriers.⁴⁷ Herein, DiD, as a drug surrogate was coloaded with PTX into the CNM3 and CCM3 for the optical animal imaging studies to probe the biodistribution of the nanotherapeutics. The particle sizes of the fluorescent micelles were detected to be 16 nm before and after photo-cross-linking (Supporting Information Figure S14). As shown in Figure 8A, the in vivo tumor imaging revealed that the nanotherapeutics could deliver much higher payload to tumor sites compared with the free dye injection. It was interesting that the specific accumulations on the spotted wound skin were observed on the male mice bearing xenografted tumors and treated with nanoformulations. It might indicate that these nanoformulations could also target the angiogenesis and inflammations in the regenerated scarring tissues by bite. Figure 8B indicated that cross-linked CCM3 formulation could deliver the highest dose of fluorescent molecules and continuously accumulate drug to tumor sites with the peak intensity between 24 and 48 h. However, the non-cross-linked CNM3 deliver relatively lower

doses of payload to the tumor site, with the signal decay (washed out) after 8 h. The ex vivo images of the tumors and different organs at 72 h in Figure 8C showed that free DiD injection led to 2- to 5-fold higher accumulation in liver, spleen, and lung relative to the intensity at tumor site (Figure 8D). In contrast, nanoformulations specifically targeted tumor site other than normal organs. Quantitative analysis of the average fluorescent intensity in Figure 8D showed more than 5-fold higher intensity of CCM3 formulation in tumor than in other normal organs, whereas about 3-fold of tumor/organ ratios were detected for the CNM3 nanoformulation. The preferred tumor uptake of CNM3 and CCM3 in female mice bearing HT-29 colon cancer xenografts were also similarly observed as shown in Supporting Information Figure S15. In addition, the PTX-DiD coloaded CCM3 also showed better tumor targeting and less nonspecific uptake than CNM3 in the SKOV-3 ovarian cancer bearing animal models (Supporting Information Figure S16).

Given the enhanced tumor-targeted drug delivery via EPR effects, these photo-cross-linked micelles CCM3 loaded with PTX may yield better anticancer efficacy *in vivo* in combination with the unaffected drug diffusion from nanoparticle within the tumor extracellular space and the accelerated drug release via S–S bond cleavage and micelle dissociation within the tumor intracellular reducing microenvironment after tumor cell uptake of the nanotherapeutics. In addition, aromatic hydrophobic anticancer drugs could be encapsulated in the coumarin-enriched core structure. For example, curcumin could be efficiently loaded in CCM3 and CCM4 at 10:1 polymer/drug ratio with the homogeneous particle sizes of 14 and 18 nm, respectively, as shown in Supporting Information Figure S17. In addition, doxorubicin could be loaded into CNM3 and CCM3 efficiently with particle sizes of 11–13 nm (Supporting Information Figure S18). The anticancer effects of the drug-loaded CCM3 will be evaluated in the near future. Although the photoinduced micelle cross-linking is a very attractive approach, one should be alerted for the possible UV damage to the drug molecules to be delivered. As we observed, PTX remained the activity after about 1 min UV exposure for micelle cross-linking. However, SN38 was observed to change color and partially lost activity after UV irradiation (>310 nm) for minutes (data is not shown).

CONCLUSIONS

In summary, we have designed and synthesized a reversibly cross-linked micelle system via combining the clean photo-cross-linking and the redox sensitive de-cross-linking of nanocarrier for effective tumor-targeted drug delivery. The fine-tuning of the telodendrimer architectures via introducing amphiphilic CA at the adjacent α -amino and conjugating coumarin on the ε -amino on polylysine via a disulfide bond-containing spacer, resulted in a spatially preferred architecture for self-assemble into efficient nanocarriers with better drug loading capacity and stability. Coumarin moieties could respond to photoirradiation reversibly to cross-link and de-cross-link nanocarriers under UV with different wavelengths. Photo-cross-linking of the micelle core structures has been demonstrated to increase the mechanical stability of telodendrimer micelles efficiently under harsh micelle-dissociating conditions *in vitro*, which were used to predict the *in vivo* micelle stability. It was surprising that the core-cross-linking of telodendrimer micelles did not alter the drug release rate in a static dialysis assay, which could be explained by a possible segregation of drug molecules and cholic acid segments from the interior cross-linked

coumarin core (Figure 6). However, CCM could reduce the toxic side effects via stable drug encapsulation during the temporary incubation with cells; yet it exhibited the similar effective anticancer effects during the continuous drug exposure in cell culture. Small animal optical imaging studies indicated the moderate improved tumor targeted drug delivery for CCM, although not significant ($p > 0.05$) than CNM formulation in tumor xenograft models via EPR effects. In addition, much less nonspecific uptakes of CCM nanoformulations were observed in normal organs than those of CNM in all three types of cancer models because of the improved mechanical stability of the cross-linked CCMs. On the basis of the above results, both enhanced mechanical stability of nanoparticle and the sustained drug release need to be achieved at the same time to further optimize the tumor targeted drug delivery. Therefore, the shell-cross-linking or intermediate layer-cross-linking of telodendrimer micelles might increase micelle stability and limit the drug diffusion to minimize premature drug release. In combination with the redox sensitive disulfide-bond cleavage for micelle de-cross-linking after uptake by tumor cells, it may further enhance the anticancer effects, which is currently under investigation.

ASSOCIATED CONTENT

Supporting Information

Route of chemical synthesis, NMR spectra, UV-vis absorption, particle sizes, and extra animal images. This material is available free of charge via the Internet at <http://pubs.acs.org>.

AUTHOR INFORMATION

Corresponding Author

*E-mail: luoj@upstate.edu. Fax: 1-315-464-5143.

Notes

The authors declare no competing financial interest.

ACKNOWLEDGMENTS

We greatly acknowledge Prof. Stephan Wilkens for assistance in TEM analysis. The authors also thank Ms. Maria Popescu for proof reading the manuscript. The financial supports from NIH/NCI R01CA140449 (Luo), Carol M. Baldwin Breast Cancer Research Foundation (Luo), and the institutional startup funds are greatly acknowledged.

REFERENCES

- (1) Davis, M. E.; Chen, Z. G.; Shin, D. M. Nanoparticle Therapeutics: An Emerging Treatment Modality for Cancer. *Nat. Rev. Drug Discovery* **2008**, *9*, 771–82.
- (2) Peer, D.; Karp, J. M.; Hong, S.; Farokhzad, O. C.; Margalit, R.; Langer, R. Nanocarriers as an Emerging Platform for Cancer Therapy. *Nat. Nanotechnol.* **2007**, *12*, 751–760.
- (3) Shi, J.; Xiao, Z.; Kamaly, N.; Farokhzad, O. C. Self-Assembled Targeted Nanoparticles: Evolution of Technologies and Bench to Bedside Translation. *Acc. Chem. Res.* **2011**, *10*, 1123–1134.
- (4) Zhang, L.; Gu, F. X.; Chan, J. M.; Wang, A. Z.; Langer, R. S.; Farokhzad, O. C. Nanoparticles in Medicine: Therapeutic Applications and Developments. *Clin. Pharmacol. Ther.* **2008**, *5*, 761–9.
- (5) Kedar, U.; Phutane, P.; Shidhaye, S.; Kadam, V. Advances in Polymeric Micelles for Drug Delivery and Tumor Targeting. *Nanomedicine (N. Y., NY, U. S.)* **2010**, *6*, 714–729.
- (6) Yokoyama, M. Polymeric Micelles as a New Drug Carrier System and Their Required Considerations for Clinical Trials. *Expert Opin. Drug Delivery* **2010**, *2*, 145–158.
- (7) Hobbs, S. K.; Monsky, W. L.; Yuan, F.; Roberts, W. G.; Griffith, L.; Torchilin, V. P.; Jain, R. K. Regulation of Transport Pathways in Tumor

- Vessels: Role of Tumor Type and Microenvironment. *Proc. Natl. Acad. Sci. U. S. A.* **1998**, *8*, 4607–12.
- (8) Maeda, H.; Wu, J.; Sawa, T.; Matsumura, Y.; Hori, K. Tumor Vascular Permeability and the EPR Effect in Macromolecular Therapeutics: A Review. *J. Controlled Release* **2000**, *1–2*, 271–84.
- (9) Jain, R. K.; Stylianopoulos, T. Delivering Nanomedicine to Solid Tumors. *Nat. Rev. Clin. Oncol.* **2010**, *11*, 653–64.
- (10) Wei, A.; Mehtala, J. G.; Patri, A. K. Challenges and Opportunities in the Advancement of Nanomedicines. *J. Controlled Release* **2012**, *2*, 236–246.
- (11) Shao, Y.; Huang, W.; Shi, C.; Atkinson, S. T.; Luo, J. Reversibly Crosslinked Nanocarriers for on-Demand Drug Delivery in Cancer Treatment. *Ther. Delivery* **2012**, *12*, 1409–1427.
- (12) Shuai, X.; Merdan, T.; Schaper, A. K.; Xi, F.; Kissel, T. Core-Cross-Linked Polymeric Micelles as Paclitaxel Carriers. *Bioconjugate Chem.* **2004**, *3*, 441–448.
- (13) Zhang, L.; Nguyen, T. L. U.; Bernard, J.; Davis, T. P.; Barner-Kowollik, C.; Stenzel, M. H. Shell-Cross-Linked Micelles Containing Cationic Polymers Synthesized Via the Raft Process: Toward a More Biocompatible Gene Delivery System. *Biomacromolecules* **2007**, *9*, 2890–2901.
- (14) Xu, X.; Smith, A. E.; Kirkland, S. E.; McCormick, C. L. Aqueous Raft Synthesis of pH-Responsive Triblock Copolymer MPEO-PAPMA-PDPAEMA and Formation of Shell Cross-Linked Micelles. *Macromolecules* **2008**, *22*, 8429–8435.
- (15) Huang, H.; Remsen, E. E.; Kowalewski, T.; Wooley, K. L. Nanocages Derived from Shell Cross-Linked Micelle Templates. *J. Am. Chem. Soc.* **1999**, *121*, 3805–3806.
- (16) Huang, H.; Wooley, K. L.; Schaefer, J. Redox Determination of the Composition of Shell Cross-Linked Amphiphilic Core–Shell Nanoparticles and the Partitioning of Sequestered Fluorinated Guests. *Macromolecules* **2001**, *3*, 547–551.
- (17) Cajot, S.; Lautram, N.; Passirani, C.; Jerome, C. Design of Reversibly Core Cross-Linked Micelles Sensitive to Reductive Environment. *J. Controlled Release* **2011**, *1*, 30–6.
- (18) Zhang, S.; Zhao, Y. Rapid Release of Entrapped Contents from Multi-Functionalizable, Surface Cross-Linked Micelles Upon Different Stimulation. *J. Am. Chem. Soc.* **2010**, *132*, 10642–4.
- (19) Koo, A. N.; Lee, H. J.; Kim, S. E.; Chang, J. H.; Park, C.; Kim, C.; Park, J. H.; Lee, S. C. Disulfide-Cross-Linked PEG-Poly(Amino Acid)S Copolymer Micelles for Glutathione-Mediated Intracellular Drug Delivery. *Chem. Commun.* **2008**, *48*, 6570–2.
- (20) Kato, J.; Li, Y.; Xiao, K.; Lee, J. S.; Luo, J.; Tuscano, J. M.; O'Donnell, R. T.; Lam, K. S. Disulfide Cross-Linked Micelles for the Targeted Delivery of Vincristine to B-Cell Lymphoma. *Mol. Pharmaceutics* **2012**, *6*, 1727–35.
- (21) Li, Y.; Xiao, K.; Luo, J.; Xiao, W.; Lee, J. S.; Gonik, A. M.; Kato, J.; Dong, T. A.; Lam, K. S. Well-Defined, Reversible Disulfide Cross-Linked Micelles for on-Demand Paclitaxel Delivery. *Biomaterials* **2011**, *27*, 6633–45.
- (22) Li, Y.; Xiao, W.; Xiao, K.; Berti, L.; Luo, J.; Tseng, H. P.; Fung, G.; Lam, K. S. Well-Defined, Reversible Boronate Crosslinked Nanocarriers for Targeted Drug Delivery in Response to Acidic pH Values and Cis-Diols. *Angew. Chem., Int. Ed.* **2012**, *12*, 2864–9.
- (23) Zhao, Y. Photocontrollable Block Copolymer Micelles: What Can We Control? *J. Mater. Chem.* **2009**, *28*, 4887–4895.
- (24) Zhao, Y. Light-Responsive Block Copolymer Micelles. *Macromolecules* **2012**, *9*, 3647–3657.
- (25) Gohy, J. F.; Zhao, Y. Photo-Responsive Block Copolymer Micelles: Design and Behavior. *Chem. Soc. Rev.* **2013**, *17*, 7117–29.
- (26) Jiang, J.; Qi, B.; Lepage, M.; Zhao, Y. Polymer Micelles Stabilization on Demand through Reversible Photo-Cross-Linking. *Macromolecules* **2007**, *4*, 790–792.
- (27) Kumar, S.; Allard, J.-F.; Morris, D.; Dory, Y. L.; Lepage, M.; Zhao, Y. Near-Infrared Light Sensitive Poly peptide Block Copolymer Micelles for Drug Delivery. *J. Mater. Chem.* **2012**, *15*, 7252–7257.
- (28) Yan, B.; Boyer, J.-C.; Branda, N. R.; Zhao, Y. Near-Infrared Light-Triggered Dissociation of Block Copolymer Micelles Using Upconverting Nanoparticles. *J. Am. Chem. Soc.* **2011**, *49*, 19714–19717.
- (29) Cheng, R.; Meng, F.; Deng, C.; Klok, H.-A.; Zhong, Z. Dual and Multi-Stimuli Responsive Polymeric Nanoparticles for Programmed Site-Specific Drug Delivery. *Biomaterials* **2013**, *14*, 3647–3657.
- (30) Raghupathi, K. R.; Azagarsamy, M. A.; Thayumanavan, S. Guest-Release Control in Enzyme-Sensitive, Amphiphilic-Dendrimer-Based Nanoparticles through Photochemical Crosslinking. *Chem. - Eur. J.* **2011**, *42*, 11752–60.
- (31) Yesilyurt, V.; Ramireddy, R.; Thayumanavan, S. Photoregulated Release of Noncovalent Guests from Dendritic Amphiphilic Nano-containers. *Angew. Chem., Int. Ed.* **2011**, *13*, 3038–42.
- (32) Fairbanks, B. D.; Singh, S. P.; Bowman, C. N.; Anseth, K. S. Photodegradable, Photoadaptable Hydrogels Via Radical-Mediated Disulfide Fragmentation Reaction. *Macromolecules* **2011**, *8*, 2444–2450.
- (33) Scott, T. F.; Schneider, A. D.; Cook, W. D.; Bowman, C. N. Photoinduced Plasticity in Cross-Linked Polymers. *Science* **2005**, *5728*, 1615–7.
- (34) Han, D.; Tong, X.; Zhao, Y. Block Copolymer Micelles with a Dual-Stimuli-Responsive Core for Fast or Slow Degradation. *Langmuir* **2012**, *5*, 2327–31.
- (35) Xuan, J.; Han, D.; Xia, H.; Zhao, Y. Dual-Stimuli-Responsive Micelle of an ABC Triblock Copolymer Bearing a Redox-Cleavable Unit and a Photocleavable Unit at Two Block Junctions. *Langmuir* **2014**, *30* (1), 410–7.
- (36) Baek, H. G.; Liu, R.; Lam, K. S. Development of Hydrogel Tentagel Shell-Core Beads for Ultrahigh Throughput Solution-Phase Screening of Encoded Oboc Combinatorial Small Molecule Libraries. *J. Comb. Chem.* **2009**, *1*, 91–102.
- (37) Luo, J.; Xiao, K.; Li, Y.; Lee, J. S.; Shi, L.; Tan, Y. H.; Xing, L.; Holland Cheng, R.; Liu, G. Y.; Lam, K. S. Well-Defined, Size-Tunable, Multifunctional Micelles for Efficient Paclitaxel Delivery for Cancer Treatment. *Bioconjugate Chem.* **2010**, *7*, 1216–1224.
- (38) Huang, W.; Shi, C.; Shao, Y.; Lam, K. S.; Luo, J. The Core-Inversible Micelles for Hydrophilic Drug Delivery. *Chem. Commun.* **2013**, *59*, 6674–6.
- (39) Xiao, K.; Luo, J.; Fowler, W. L.; Li, Y.; Lee, J. S.; Xing, L.; Cheng, R. H.; Wang, L.; Lam, K. S. A Self-Assembling Nanoparticle for Paclitaxel Delivery in Ovarian Cancer. *Biomaterials* **2009**, *30*, 6006–16.
- (40) Xiao, K.; Li, Y.; Luo, J.; Lee, J. S.; Xiao, W.; Gonik, A. M.; Agarwal, R. G.; Lam, K. S. The Effect of Surface Charge on in Vivo Biodistribution of Peg-Oligocholic Acid Based Micellar Nanoparticles. *Biomaterials* **2011**, *13*, 3435–46.
- (41) Xiao, K.; Li, Y.; Lee, J. S.; Gonik, A. M.; Dong, T.; Fung, G.; Sanchez, E.; Xing, L.; Cheng, H. R.; Luo, J.; Lam, K. S. “OaO2” Peptide Facilitates the Precise Targeting of Paclitaxel-Loaded Micellar Nanoparticles to Ovarian Cancer in Vivo. *Cancer Res.* **2012**, *8*, 2100–10.
- (42) He, J.; Zhao, Y.; Zhao, Y. Photoinduced Bending of a Coumarin-Containing Supramolecular Polymer. *Soft Matter* **2009**, *2*, 308–10.
- (43) Trenor, S. R.; Shultz, A. R.; Love, B. J.; Long, T. E. Coumarins in Polymers: From Light Harvesting to Photo-Cross-Linkable Tissue Scaffolds. *Chem. Rev.* **2004**, *6*, 3059–77.
- (44) Chen, Y.; Chou, C.-F. Reversible Photodimerization of Coumarin Derivatives Dispersed in Poly(Vinyl Acetate). *J. Polym. Sci., Part A: Polym. Chem.* **1995**, *16*, 2705–14.
- (45) Britten, R. A.; Green, J. A.; Warenius, H. M. Cellular Glutathione (GSH) and Glutathione S-Transferase (GST) Activity in Human Ovarian Tumor Biopsies Following Exposure to Alkylating Agents. *Int. J. Radiat. Oncol. Biol. Phys.* **1992**, *3*, 527–31.
- (46) Balendiran, G. K.; Dabur, R.; Fraser, D. The Role of Glutathione in Cancer. *Cell. Biochem. Funct.* **2004**, *6*, 343–52.
- (47) Bastiat, G.; Pritz, C. O.; Roider, C.; Fouchet, F.; Lignieres, E.; Jesacher, A.; Glueckert, R.; Ritsch-Marte, M.; Schrott-Fischer, A.; Saulnier, P.; Benoit, J. P. A New Tool to Ensure the Fluorescent Dye Labeling Stability of Nanocarriers: A Real Challenge for Fluorescence Imaging. *J. Controlled Release* **2013**, *3*, 334–42.